



THE UNIVERSITY *of* EDINBURGH

## Edinburgh Research Explorer

### CO<sub>2</sub> adsorption on different organo--modified SBA--15 silicas: a multidisciplinary study on the effects of basic surface groups

**Citation for published version:**

Gatti, G, Costenaro, D, Vittoni, C, Paul, G, Crocella, V, Mangano, E, Brandani, S, Bordiga, S, Cossi, M, Marchese, L & C, B 2017, 'CO<sub>2</sub> adsorption on different organo--modified SBA--15 silicas: a multidisciplinary study on the effects of basic surface groups', *Physical Chemistry Chemical Physics*, pp. 14114-14128.  
<https://doi.org/10.1039/C6CP08048K>

**Digital Object Identifier (DOI):**

[10.1039/C6CP08048K](https://doi.org/10.1039/C6CP08048K)

**Link:**

[Link to publication record in Edinburgh Research Explorer](#)

**Document Version:**

Peer reviewed version

**Published In:**

Physical Chemistry Chemical Physics

**General rights**

Copyright for the publications made accessible via the Edinburgh Research Explorer is retained by the author(s) and / or other copyright owners and it is a condition of accessing these publications that users recognise and abide by the legal requirements associated with these rights.

**Take down policy**

The University of Edinburgh has made every reasonable effort to ensure that Edinburgh Research Explorer content complies with UK legislation. If you believe that the public display of this file breaches copyright please contact [openaccess@ed.ac.uk](mailto:openaccess@ed.ac.uk) providing details, and we will remove access to the work immediately and investigate your claim.





## CO<sub>2</sub> adsorption on different organo-modified SBA-15 silicas: a multidisciplinary study on the effects of basic surface groups

G. Gatti,<sup>a\*</sup> D. Costenaro,<sup>a</sup> C. Vittoni,<sup>a</sup> G. Paul,<sup>a</sup> V. Crocellà,<sup>b</sup> E. Mangano,<sup>c</sup> S. Brandani,<sup>c</sup> S. Bordiga,<sup>b</sup> M. Cossi,<sup>a</sup> L. Marchese<sup>a</sup> and C. Bisio<sup>a,d\*</sup>

Received 00th January 20xx,  
Accepted 00th January 20xx

DOI: 10.1039/x0xx00000x

www.rsc.org/

A Hybrid organic-inorganic SBA-15 silicas functionalized with increasing amounts of amino groups were studied in this work aiming to evaluate the effects of their physico-chemical properties on CO<sub>2</sub> capture ability. Three different amino-silane species were used: 3-aminopropyltriethoxysilane (APTS), 3-(2-aminoethyl) aminopropyltrimethoxysilane (EAPTS) and 3-[2-(2-aminoethyl)aminoethyl] aminopropyltrimethoxysilane (PAPTS). More specifically, samples were prepared by using two methods, following a post-synthesis grafting procedure and a one-pot preparation method. Experimental and computational techniques were used study structural and textural properties of obtained samples and their surface species in relation to the adopted preparation method. For the most reactive samples, additional hints on the interactions of organosilane species with the silica surface were obtained by a combination of IR and SS-NMR spectroscopy, with particular emphasis to the effects of the silane chain length on the mobility of the organic species. Advanced complementary solid-state NMR techniques provided deeper information on the interactions of organosilane species with the silica surface. Finally, the amount of CO<sub>2</sub> adsorbed was estimated comparing classical microcalorimetric analysis method with a new type of screening test, the Zero-Length Column analysis, that is able to evaluate on a small amount of samples in a very short time the adsorption properties of the adsorbents. The reactivity of the amino-modified silica samples is deeply influenced by both the preparation route and by the type of organosilane used for the functionalization of the materials. In particular, samples prepared by the post-synthesis grafting procedure and containing higher amount of amino groups in the chain are more reactive, following the order PAPTS > EAPTS > APTS.

### Introduction

In recent decades, the atmospheric concentration of CO<sub>2</sub> has largely increased in relation to anthropogenic causes thus contributing to the global warming (Greenhouse Effect). In order to reduce the amount of CO<sub>2</sub> released to the atmosphere, several methods of Carbon Capture and Storage (CCS) have been proposed in the literature.<sup>1</sup> Three main categories of CO<sub>2</sub> capture technologies include: i) post-combustion, ii) pre-combustion, and iii) oxy-fuel combustion methods. In this respect, the most mature, green and cheap method are based on post-combustion CO<sub>2</sub> capture processes.<sup>2</sup> Among the available methods, the CO<sub>2</sub> wet absorption (i.e. liquid phase absorption in amine solutions) is currently one of the most used technologies, although it presents several

disadvantages such as the large amount of energy requested for the regeneration, corrosion of the apparatus and volatility of the employed solutions.<sup>3</sup> In order to overcome these problems, a promising approach that has attracted great attention is the CO<sub>2</sub> capture using solid sorbents. This technology seems to be associated to positive environmental effects and energy efficiency.<sup>4</sup> Several types of solid sorbents have been proposed. In particular, materials working through physisorption (i.e. zeolites, activated carbon, MOFs and porous polymers as COFs, CTFs and PAFs) or chemisorption processes (i.e. lithium/sodium/potassium based sorbents, calcium oxides, hydrotalcites or amine supported materials) are currently studied.<sup>5,6,7,8,9</sup> Among these materials, organic-inorganic hybrid samples show potential applications as CO<sub>2</sub> adsorbents, owing to their high adsorption capacity, high selectivity, and excellent chemical stability.<sup>1</sup> Among these porous solids functionalized with amino groups deserve particular attention in relation to the encouraging results. These materials can be prepared by incorporation of different organic compounds containing amino groups (i.e. through grafting of aminosilanes or impregnation of monomers and polymers as polyethylenimine<sup>10</sup>) on the surface of supporting materials.<sup>11</sup>

As a general feature, the interaction of CO<sub>2</sub> with primary and secondary amines leads to the formation of carbamates and carbamic acid species.<sup>12</sup> It is proposed in many publications that the reaction is governed by several different mechanisms.<sup>13,14</sup> At first,

<sup>a</sup> Dipartimento di Scienze e Innovazione Tecnologica and "Centro interdisciplinare Nano-SiSTeMI", Università del Piemonte Orientale, via T. Michel 11, 15121 Alessandria, Italy.

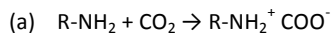
<sup>b</sup> Department of Chemistry, NIS and INSTM Reference Centres, University of Turin, I-10135 Torino, Italy.

<sup>c</sup> Scottish Carbon Capture and Storage, School of Engineering, University of Edinburgh, Mayfield Road, Edinburgh, EH9 3JL, U.K.

<sup>d</sup> ISTM-CRN Istituto di Scienze e Tecnologie Molecolari, via G. Venezian 21, Milano, Italy.

Electronic Supplementary Information (ESI) available: [details of any supplementary information available should be included here]. See DOI: 10.1039/x0xx00000x

the terminal amino group of the alkyl chain can react with the CO<sub>2</sub> forming a zwitterionic intermediate (a). The following two ways are possible for the zwitterionic intermediate: i) a rearrangement with the consequent formation of carbamic acid (b1); ii) an interaction with a free base such as water, hydroxyl groups of silanols or another amine, forming an alkylammonium carbamate species (b2).



In dry conditions, if the organic chain contains only one amino group, the reaction takes place via intermolecular mechanism. This involves an amine group of another molecule, if the silane density is high and the organic chains are close enough, or a silanol group of the silica surface. If, on the other hand, the alkyl chain contains another amino group, the base B is present in the same molecule, and therefore the reaction can also occur via intramolecular mechanism.<sup>15</sup>

Ordered porous silica-based materials like HMS, mesoporous silica microspheres, mesocellular silica foam, MCM-41, MCM-48, SBA-12, SBA-15, SBA-16 and KIT-6, have been widely investigated as solid sorbent for CO<sub>2</sub> capture.<sup>11</sup> In fact, they are good candidates for CO<sub>2</sub> capture for their structural and textural properties, such as large pore size, high specific surface area and pore volume. All these properties facilitate a good dispersion of basic amino groups on the surface, thus increasing CO<sub>2</sub> adsorption capacity.<sup>16</sup>

Compared to the other mesoporous materials, SBA-15 was found to be one of the most suitable substrates for CO<sub>2</sub> capture thanks to its large pore volume and diameter.<sup>5</sup> Additionally, the intra-wall pores of SBA-15 form a continuous network that connects adjacent channels, which promotes the mass transfer during the adsorption. This facilitates the interaction between the CO<sub>2</sub> and the amino groups and the resulting formation of carbamate groups.<sup>17</sup>

Different studies of CO<sub>2</sub> adsorption on SBA-15 silica containing amino species are reported in the literature. For example, Wang et al.<sup>3</sup> have grafted SBA-15 silica with 3-aminopropyltrimethoxysilane obtaining a material with CO<sub>2</sub> uptake of ca. 1.59 mol/kg at 25 °C and 0.15 atm), while Chang et al.<sup>18</sup> used as grafting agent 3-trimethoxysilylpropyl diethylenetriamine that exhibited a CO<sub>2</sub> adsorption capacity of 2.41 mol/kg adsorbent, (60 °C, 0.15 atm).

Even if several studies in the literature reported the use of silanes with different concentration of basic species, the CO<sub>2</sub> capture performances of these materials is difficult to be compared in that in many cases different conditions of pressure and temperature have been adopted.

Recently, Yoo et al.<sup>15</sup> compared SBA-15 functionalized with amine-containing organosilanes with different chain length (including 3-aminopropyltrimethoxysilane (APTS), 3-(2-aminoethyl)aminopropyltrimethoxysilane (EAPTS) and 3-[2-(2-aminoethyl)aminoethyl] aminopropyltrimethoxysilane (PAPTS)) with low loading of silane adsorbents (~0.45 mmol silane/g). In their work, particularly focused on the determination of CO<sub>2</sub> adsorption mechanism with functionalized silica surface, they suggested the occurrence of intramolecular mechanism for CO<sub>2</sub>

adsorption on EAPTS and PAPTS, whereas for samples grafted with shorter silane species (APTS) an intermolecular mechanism was proposed. The key-role of silanol groups in CO<sub>2</sub> interactions was also enlightened.

In our work, hybrid organic-inorganic SBA-15 materials functionalized with high loading of APTS, EAPTS and PAPTS were prepared by using both post-synthesis and one-pot methods, aiming to determine the effect of the synthesis procedure on the CO<sub>2</sub> adsorption processes. It is known indeed that materials prepared by one-pot methods have a more homogenous distribution of organic species and, in general, the amount of incorporated functional species is higher with respect to samples prepared by post-synthesis method<sup>19</sup>. To our knowledge, SBA-15 related samples functionalized via one-pot procedure with EAPTS and PAPTS were prepared for the first time in this work.

The structure and interactions occurring at the surface of the different hybrid organic-inorganic materials were studied by coupling experimental (mainly IR and SS-NMR spectroscopy) and computational techniques. <sup>1</sup>H Hahn echo MAS NMR was applied for the first time to have hints on the interactions between amine and surface silanols, aiming at evaluating the mobility of the chains on the SBA-15 surface, a relevant parameter that influences the adsorption performances. Ab-initio calculations were also considered to determine the structure of functionalized materials.

Adsorption of CO<sub>2</sub> on the materials was studied by different experimental techniques. Besides classical IR spectroscopy, SS-NMR, microcalorimetric analysis and Zero-Length Column Chromatography were also used. This last experimental technique is a new quantitative analysis for hybrid organic-inorganic samples, and represents a relevant screening method for prototype adsorbents because it requires small amount of samples and very short time of analysis.

## Experimental

### Materials preparation

**SBA-15 silica.** The SBA-15 mesoporous silica was prepared following the synthesis method reported by Zhao<sup>20</sup>. Pluronic P123 triblock copolymer (4.0 g, Sigma Aldrich, 435465-250ML, M.W.= 5800) was dissolved in 30 mL of deionized water in a thermostated bath at 35°C. The obtained gel was mixed with a mechanical stirrer for 24 h; after this time 120 g of 2M HCl solution was slowly added to the gel. After 1h, tetraethyl orthosilicate (TEOS) (8.5 g, Si(OC<sub>2</sub>H<sub>5</sub>)<sub>4</sub>, Sigma Aldrich, 131903-25ML, M.W. = 208.33 g/mol) was finally added. After 1 h stirring, the gel was introduced in a Teflon autoclave (125 mL capacity, Anton PAAR 4748) and heated at 100°C for 24 h. At the end of this procedure, samples were filtered, washed with 2L of deionized water and dried for 36 h at 120°C. The material was then calcined under air flow (100 mL/min) at 550°C for 5 h (heating ramp 1°C/min) in order to remove the organic species used as template molecules.

**Post-synthesis functionalization of SBA-15 silica.** The bare SBA-15 sample was functionalized in order to introduce amino groups on the surface by using a post-synthesis grafting procedure. Three

different organic silanes were used: 3-aminopropyltriethoxysilane (APTS), 3-(2-aminoethyl)aminopropyltrimethoxysilane (EAPTS) and 3-[2-(2-aminoethyl)aminoethyl] aminopropyltrimethoxysilane (PAPTS).

Three aliquots of 1.0 g of SBA-15 silica were treated in vacuum at 200°C for 2 h to remove physisorbed water. After this treatment, the samples were kept under N<sub>2</sub> flow and then dispersed in 100 mL of anhydrous toluene before the addition of the organic silane. In one case, 0.53 mL of 3-aminopropyltriethoxysilane [(APTS) (H<sub>2</sub>N(CH<sub>2</sub>)<sub>3</sub>Si(OCH<sub>3</sub>)<sub>3</sub>, Sigma-Aldrich, M.W.= 221.37 g/mol)] were added drop-by-drop to the SBA-15 suspension that was then left for 20 h at 50°C under magnetic stirring. After this, the sample was recovered by filtering, and the powder washed with toluene and ethyl ether to remove the unreacted silane, and finally dried for 1 night at 80°C.<sup>21</sup> This sample was hereafter named A-SBA15. For the other two SBA-15 samples, 0.49 mL of N-[3-(trimethoxysilyl)propyl]-ethylenediamine (EAPTS) (H<sub>2</sub>N(CH<sub>2</sub>)<sub>2</sub>NH(CH<sub>2</sub>)<sub>3</sub>Si(OCH<sub>3</sub>)<sub>3</sub>, Sigma-Aldrich, M.W. = 222.36 g/mol) and 0.48 mL of N-[3-(trimethoxysilyl)propyl]-diethylenetriamine (PAPTS) (H<sub>2</sub>N(CH<sub>2</sub>)<sub>2</sub>NH(CH<sub>2</sub>)<sub>2</sub>NH(CH<sub>2</sub>)<sub>3</sub>Si(OCH<sub>3</sub>)<sub>3</sub>, Sigma-Aldrich, M.W.= 265.43 g/mol) were added, respectively. The same preparation protocol adopted for A-SBA-15 was followed in the case of these samples. Recovered samples were hereafter named E-SBA-15 and P-SBA-15, respectively.

#### One-pot preparation of functionalized SBA-15 related materials.

Organo-modified SBA-15 silica samples were also prepared via one-pot synthesis by adapting the method reported by Hao et al.<sup>22</sup> In particular, Pluronic P123 triblock copolymer (2.0 g, Sigma Aldrich, 435465-250ML, M.W.= 5800) was dissolved in 15 mL of deionized water in a thermostated bath at 35°C. The obtained gel was mixed with a mechanical stirrer for 24 h; after this time 60 g of 2M HCl solution was slowly added to the gel. After 1 h, tetraethyl orthosilicate (TEOS) (3.8 g, Si(OC<sub>2</sub>H<sub>5</sub>)<sub>4</sub>, Sigma Aldrich, 131903-25ML, M.W.= 208.33 g/mol) was finally added. After the addition of TEOS the solution was stirred for two hours and then a 10 mol% of the desired organosilane (i.e. APTS, EAPTS or PAPTS) was added to the gel and stirred for 24 hours. After this time, the gel was introduced in a Teflon autoclave (125 mL capacity, Anton PAAR 4748) and heated at 100°C for 24 h. At the end of this procedure, samples were filtered, washed with 2L of deionized water and dried for 36 h at 120°C. The organic template was removed by extraction with ethanol at 80°C for 24 h. Finally, the organo-functionalized silica samples were dried again at 120°C for 16 hours. The obtained samples will be hereafter named A-SBA-15(OP), E-SBA-15(OP) and P-SBA-15(OP), respectively.

#### Characterization techniques

*X-ray diffractograms (XRD)* were collected on unoriented ground powders with a Thermo ARL 'XTRA-048 diffractometer with a CuK $\alpha$  ( $\lambda$ =1.54 Å) radiation, from 0.7 and to 3° 2 $\theta$  degrees with a step size of 0.02° 2 $\theta$  and a rate of 1° 2 $\theta$  /min.

*N<sub>2</sub> physisorption measurements* were carried out at 77 K in the relative pressure range from 10<sup>-7</sup> to 1 p/p<sub>0</sub> by using a

Quantachrome Autosorb iQ2 instrument. Before the analysis the samples were outgassed at 150°C for 3 h (residual pressure  $p < 10^{-6}$  Torr). Specific surface areas were determined by using Brunauer–Emmett–Teller equation, in the residual pressure range from 0.01 to 0.1 p/p<sub>0</sub>. Pore size distributions were obtained by applying the Non Localized Density Functional Theory (NLDFT) method (N<sub>2</sub> silica kernel based on a cylindrical pore model).

*Thermogravimetric analyses (TGA)* were performed on a Setaram SETSYS Evolution instrument under O<sub>2</sub> (gas flow rate 100 mL/min), heating the samples from 30 °C to 800°C with a rate of 5°C/min.

*C-H-N elemental contents* were determined using an EA 3000 elemental analyser (EuroVector). Helium and oxygen at 120 and 35 kPa pressure were used, respectively. For each material, three measurements were done.

*Infrared spectra* were collected on a Thermo Electron Corporation FT Nicolet 5700 Spectrometer (resolution 4 cm<sup>-1</sup>). Self-supporting pellets were placed into homemade IR cell with KBr windows permanently attached to vacuum line (residual pressure < 1x10<sup>-4</sup> mbar), allowing all treatments and adsorption-desorption experiments to be carried out in situ. Before the gas adsorption tests, the silica samples were outgassed at 135°C with a heating ramp of 5°C/min for 3 h; an oil-free apparatus and grease-free vacuum line were used. The samples were cooled at room temperature for the collection of IR spectra upon CO<sub>2</sub> adsorption. All the spectra were normalized by dividing for the density of the self-standing pellets, obtained by dividing the samples mass for the area of the pellets. The samples mass values were 0.0014 g, 0.0021 g and 0.0011 g, while the area of the pellets were 52 mm<sup>2</sup>, 67 mm<sup>2</sup> and 42 mm<sup>2</sup>, respectively for A-SBA-15, E-SBA-15 and P-SBA-15. In addition, the proper normalization of the IR spectra was verified taking as reference the intensity of the overtones and combination modes of the silica framework (bands in the 2200–1600 cm<sup>-1</sup> range). In this way, differences of the bands intensity among different samples related to intrinsic oscillators of the materials (e.g. hydroxyl groups) can be associated to actual differences in the amount of such species in the samples. As a consequence of the normalization, the absorbance values are reported as arbitrary unit (a.u.).

*Solid state NMR (SS-NMR)* spectra were acquired on a Bruker Avance III 500 spectrometer and a wide bore 11.7 Tesla magnet with operational frequencies for <sup>1</sup>H, <sup>29</sup>Si and <sup>13</sup>C of 500.13, 99.35 and 125.77 MHz, respectively. A 4mm triple resonance probe with MAS was employed in all the experiments. The samples were packed on a Zirconia rotor and spun at a MAS rate in the 0 – 15 kHz range. The magnitudes of radio frequency fields,  $\nu_{rf}$ , were 62.5 and 33.3 kHz for <sup>13</sup>C and <sup>29</sup>Si, respectively. The relaxation delays,  $d_1$ , between accumulations were 2.5, 100 and 180 s for <sup>1</sup>H, <sup>13</sup>C and <sup>29</sup>Si MAS NMR, respectively. For the <sup>13</sup>C{<sup>1</sup>H} CPMAS experiments, the radio frequency fields  $\nu_{rfH}$  of 55 and 28 kHz were used for initial excitation and decoupling, respectively. During the CP period the <sup>1</sup>H RF field  $\nu_{rfH}$  was ramped using 100 increments, whereas the <sup>13</sup>C RF field  $\nu_{rfC}$  was maintained at a constant level. During the acquisition, the protons are decoupled from the carbons by using a TPPM decoupling scheme. A moderate ramped RF field  $\nu_{rfH}$  of 62 kHz was

used for spin locking, while the carbon RF field  $\nu_{\text{rfC}}$  was matched to obtain optimal signal and the CP contact time of 2 ms was used. Rotor synchronized Hahn echo sequence ( $\pi/2-\tau-\pi-\tau$ -acquisition) was also applied to record the  $^1\text{H}$  NMR spectra with  $\tau$  delay time of 6700  $\mu\text{s}$  and  $90^\circ$  pulse length of 2.5  $\mu\text{s}$ . All chemical shifts are reported using  $\delta$  scale and are externally referenced to TMS at 0 ppm. All  $^{29}\text{Si}$  MAS NMR spectra were fitted with DMFIT functions for quantitative deconvolution of overlapping peaks.<sup>23</sup> Before the gas adsorption tests, the silica samples were outgassed at  $135^\circ\text{C}$  with a heating ramp of  $5^\circ\text{C}/\text{min}$  for 3 h; an oil-free apparatus and grease-free vacuum line were used. The samples were cooled at room temperature and 60 mbar of  $^{13}\text{CO}_2$  was placed in contact with the samples and then kept in that atmosphere for at least 2 days. After that the rotor was packed in a glove box and submitted for solid state NMR experiments. The label  $^{13}\text{CO}_2$  was used in order to increase the signal intensity.

*Microcalorimetric  $\text{CO}_2$  adsorption measurements* to calculate the heat of adsorption were carried out at  $30^\circ\text{C}$  by means of a heatflow microcalorimeter (Calvet C80, Setaram, France) connected to a grease-free high-vacuum gas-volumetric glass apparatus (residual  $p \approx 10^{-6}$  Torr) equipped with a Ceramicell 0-100 Torr gauge and a Ceramicell 0-1000 Torr gauge (by Varian), following a well established stepwise procedure, described in detail elsewhere<sup>28</sup>. This procedure allows determining, during the same experiment, both integral heats evolved ( $-Q_{\text{int}}$ ) and adsorbed amounts ( $n_{\text{a}}$ ) for very small increments of the adsorptive pressure. Adsorbed amounts and integral heats evolved, normalized to the sample mass, have been plotted vs. pressure in the form of volumetric (quantitative) and calorimetric isotherms (here not reported for the sake of brevity), respectively. The adsorption heats observed for each small dose of gas admitted over the sample ( $q_{\text{diff}}$ ) have been finally reported as a function of coverage, in order to obtain the (differential) enthalpy changes associated with the proceeding adsorption process ( $q_{\text{diff}} = -\Delta_{\text{ads}}H$ ). The differential-heat plots presented here were obtained by taking the middle point of the partial molar heats ( $\Delta Q_{\text{int}}/\Delta n_{\text{a}}$ , kJ/mol) vs  $n_{\text{a}}$  histogram relative to the individual adsorptive doses. Before the quantitative/calorimetric measurement, all materials were activated in vacuum at  $150^\circ\text{C}$  for 3 hours. In all experiments, after the first adsorption run carried out on the activated samples (the primary isotherm), samples were outgassed overnight at the adsorption temperature ( $30^\circ\text{C}$ ), and then a second adsorption run was performed (the secondary isotherm), in order to check whether secondary and primary adsorption runs coincided, or an irreversible adsorbed fraction was present.

*The Zero Length Colum* consists in a  $1/8''$  Swagelok union in which a very small amount of sample (10–15 mg) is placed as monolayers between two sister discs. The method was originally introduced to measure the intra-particle diffusion of hydrocarbons in zeolites<sup>24</sup> and, more recently it has been extended to the screening of the adsorption properties of novel adsorbents for  $\text{CO}_2$  capture.<sup>25,26</sup> The experiment is based on following the desorption curve of a sample previously equilibrated with a known mixture at constant flow rate. For the characterization of adsorbents for post-combustion capture

the feed mixture is composed by 10%  $\text{CO}_2$  in He. Once the equilibrium is reached the inlet flow to the ZLC is switched to pure He (carrier) and the desorption starts. The system is equipped with drying columns to ensure the removal of any traces of water from the gases entering the system. The concentration in the gas phase is monitored using a Dycor Ametek Benchtop quadrupole mass spectrometer connected to the outlet of the ZLC. Full details of the system used for these experiments are given in an earlier publication.<sup>26</sup> For this study the amount of sample packed in the ZLC were: SBA-15 (2.4 mg), A-SBA-15 (3.5 mg), E-SBA-15 (5.9 mg), and P-SBA-15 (7.3 mg).

Prior each experiment the samples were regenerated overnight at  $150^\circ\text{C}$  under He flow. Each experiment was carried out at two different flow rates, 2 and 2.7 ml/min, to check if the sample are equilibrium or kinetically controlled.<sup>27</sup> To ensure that complete equilibrium was achieved ZLC experiment were repeated at increasing adsorption times. The system was considered at equilibrium when the  $\text{CO}_2$  uptake did not change any more with the adsorption time. According to this procedure the resulting equilibration time for A-SBA-15 was 40 min while for E-SBA-15 and P-SBA-15 the adsorption time required was 20 min. *Theoretical calculations* have been performed with Gaussian09 program at the Density Functional Theory (DFT) level, with hybrid functional B3LYP<sup>29,30,31</sup>, using Dunning's correlation-consistent cc-PVDZ basis set on light atoms,<sup>32,33</sup> and LANL2DZ effective core potentials and basis set for silicon.<sup>34</sup> The atom-atom pairwise algorithm proposed by Grimme<sup>35</sup> and implemented in Gaussian09 was used to estimate the contribution from dispersion (van der Waals) forces to energies and geometrical structures.

The silica surface was simulated by two cluster models, with  $\text{Si}_3\text{9O}_{112}\text{H}_{68}$  (I) and  $\text{Si}_2\text{0O}_{152}\text{H}_{92}$  (II) stoichiometry: the models have a surface of approximately 2.5 and 4  $\text{nm}^2$ , respectively; hydrogen atoms were added to saturate the oxygen valences at the cluster border and on the "external" surface. These clusters were extracted from the large model of amorphous silica optimized in literature<sup>36</sup>, dealing with MCM-14 modeling: though MCM-14 and SBA-15 differ for the mesoscopic structure, i.e. mesopore size and channel topology, at this scale the atomistic structures of their inner surfaces are fully comparable. The silanol concentration on the model surfaces, a crucial parameter to describe the interactions with the attached molecules, was set to 5  $\text{SiOH}/\text{nm}^2$ , to reproduce the experimental measures described below.

To simulate the functionalized surfaces, one to three molecules of APTS, EAPTS and PAPTS were grafted to cluster I and II surfaces by eliminating three water molecules from silanol groups, and thus forming three Si-O-Si bonds per each chain; when more than one molecule were added, a homogeneous distribution of chains attached to the surface was assumed.

## Results and Discussion

### Physico-chemical properties of organo-modified SBA-15 silicas

The structural properties of hybrid organic-inorganic SBA-15 samples prepared by post-synthesis grafting and one pot method were studied by XRD analysis (figure 1).

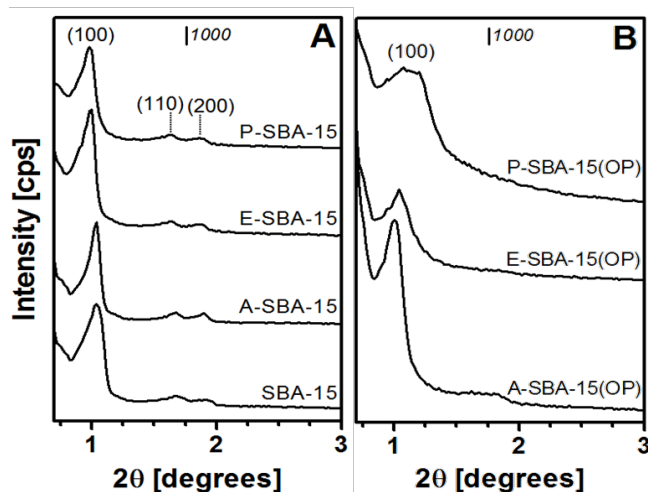


Fig. 1. XRD pattern of pure SBA-15 material and post-synthesis grafted samples (frame A) and SBA-15 related materials prepared by one-pot method (frame B).

Pure SBA-15 silica sample after calcination to remove the polymer template (figure 1A) shows reflections at  $0.9$ ,  $1.5$  e  $1.8^\circ 2\theta$ , corresponding to (100), (110) and (200) planes typical of hexagonally ordered mesoporous silica.<sup>20, 37</sup> All samples in figure 1A show the same reflections indicating that, as expected, the process of grafting did not modify the ordered structure typical of these materials. Diffraction pattern of samples prepared by one-pot method are reported in figure 1B. A-SBA-15 (OP) sample is characterized by the presence of (100) reflection at ca.  $0.9^\circ 2\theta$  and a broad signal in the  $1.5$ – $2^\circ 2\theta$  range where reflections related to (110) and (200) planes are probably merged. Samples prepared with silanes with longer chains (i.e. EAPTS and PAPTS) appeared less organized with respect to A-SBA-15 (OP), as indicated by the presence of the a single and broad reflection related to the (100) plane. This suggests that the use of silanes with longer chains for the synthesis of mesoporous materials led to a more disordered mesoporous structure. One-pot samples were also studied by TEM in order to have direct information on pores arrangement (figure S1 in Supplementary Material). The A-SBA-15 (OP) and E-SBA-15 (OP) samples are characterized by a well organized hexagonal arrangement of pores (even if in the latter sample appeared less ordered), whereas the porous architecture of P-SBA-15 (OP) material is more disordered, in agreement with XRD analysis.

$N_2$  physisorption at 77K analysis was carried out to collect information on the textural properties of grafted and one-pot prepared samples, with special consideration to the determination

of specific surface area and pore size distribution. In particular, pore size distribution of obtained samples is reported in figure 2.

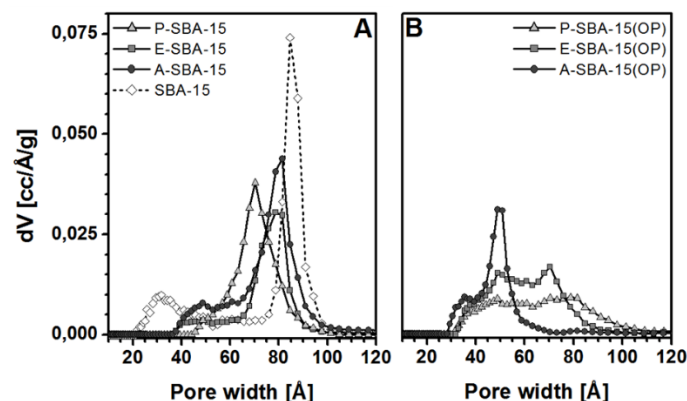


Fig. 2. Pore size distribution (determined by  $N_2$  physisorption at 77K applying NLDFT methods) of grafted samples compared to parent SBA-15 material (frame A) and one-pot synthesized materials (frame B).

All samples (both prepared by one-pot method and post-synthesis grafting) show type IV adsorption isotherms based on the IUPAC classification, indicating the presence of mesoporosity in the materials. For all grafted samples can be observed an H1 hysteresis loop typical of materials with cylindrical pore (figure S2 in the Supplementary Material).<sup>38</sup> The BET method was used to estimate the specific surface area (S.S.A.) of the solids. The bare SBA-15 silica shows a S.S.A. of  $720 \text{ m}^2/\text{g}$ , whereas a progressive decrease of S.S.A. for the grafted silica samples was observed as a function of the silane chain length:  $563$ ,  $360$  and  $236 \text{ m}^2/\text{g}$  for the samples A-SBA-15, E-SBA-15 and P-SBA-15, respectively (Table 1). The reduction of specific surface area should be ascribed to the presence of the organic species that limits the entrance to the SBA-15 pores: the longer is the silane chain length, the stronger is the pore blocking effect.<sup>39</sup> The A-SBA-15(OP) sample is characterized by hysteresis loops of H2a type (following new IUPAC definition<sup>40</sup>) suggesting the presence of more disordered pores with respect to the analogous grafted samples. The shape of the isotherm suggested complex pore architecture in which pore blocking and percolations effects can be postulated (figure S2 in the Supplementary Material). Also the E-SBA-15(OP) and P-SBA-15(OP) samples show hysteresis loops of H2a type, thus indicating the presence of materials with disordered pores and larger pore. Specific surface area (SSA) of one-pot prepared samples progressively decrease from A-SBA-15(OP) to P-SBA-15(OP), passing from  $552$  to  $416 \text{ m}^2/\text{g}$  (Table 1). The pore size distribution of silica samples was determined by the NLDFT model using a kernel based on a cylindrical pore model related to the desorption branch of the isotherms on silica surface (figure 2). The bare silica SBA-15 sample is characterized by two families of pores, the first one with a maximum centered at ca.  $85 \text{ Å}$  and the second with dimensions from  $20$  to  $40 \text{ Å}$ , which has been assigned to pores connecting the bigger mesopores (figure 2A).<sup>41</sup> After the post-synthesis functionalization, for A-SBA-15 sample, the pore at ca.  $85 \text{ Å}$  its shift



at ca. 80 Å and a family of smaller pores located from 20 to 40 Å disappears, when a new family of pores with dimension of 40-60 Å appears. E-SBA-15 and P-SBA-15 samples have the same behavior, even if pores with dimension of 40-60 Å are less numerous and the principal pores are shifted at 80 and 70 Å respectively. The total pore volume for the SBA-15 was 0.98 cc/g whereas for A-SBA-15, E-SBA-15 and P-SBA-15 samples were 0.94, 0.57 and 0.41 cc/g, respectively. The A-SBA-15(OP) sample is characterized by two families of pores at ca. 35 and 50 Å, definitively smaller than the analogous A-SBA-15 grafted sample, whereas a larger pore distribution was found for the other two samples prepared by one-pot method. In particular, E-SBA-15(OP) sample has pores in the 30-90 Å range with two maxima at 50 and 70 Å. Finally, the P-SBA-15(OP) material showed the broadest pore distribution and disordered pores with dimensions between 30 and 110 Å (figure 2B). It can be noticed that increasing the silane length, the volume of pores centered at 50 Å decreases progressively in favor of more disordered pore structures, in good agreement with XRD and TEM analysis. Pore volume of one-pot prepared samples is reported in Table 1.

Table 1. Specific Surface Area (S.S.A.), total pore volume (V<sub>p</sub>), nitrogen and silane concentrations of both grafted (A-SBA-15, E-SBA-15 and P-SBA-15) and one-pot (A-SBA-15(OP), E-SBA-15(OP) and P-SBA-15(OP)) samples. Pure silica SBA-15 is also reported for comparison.

Sample	S. S. A. [m <sup>2</sup> /g]	V <sub>p</sub> [cc/g]	Conc. N [mmol/g] <sup>a</sup>	Conc. Silane [mmol/g] <sup>b</sup>
SBA-15	720	0.98	-	-
A-SBA-15	563	0.94	1.05	1.05
E-SBA-15	360	0.57	2.60	1.30
P-SBA-15	236	0.41	3.50	1.16
A-SBA-15(OP)	552	0.59	1.10	1.10
E-SBA-15(OP)	430	0.62	2.76	1.38
P-SBA-15(OP)	416	0.46	2.78	0.93

<sup>a</sup>Determined by elemental analysis. <sup>b</sup>Obtained by dividing the nitrogen concentration by the number of N atoms in the single silane chain.

The concentration of nitrogen atoms introduced in the samples by the different preparation procedure is reported in Table 1. It was estimated that the N content (expressed as mmol of N per g of sample) is ca. 1.05, 2.60 and 3.50 mmol/g for grafted A-SBA-15, E-SBA-15 and P-SBA-15 samples, respectively. The concentration of silane molecules on the grafted A-SBA-15, E-SBA-15 and P-SBA-15 samples was also calculated by dividing the total amine loading by 1, 2, and 3, respectively (i.e. by the number of nitrogen atoms in each silane chain). All these data are summarized in Table 1. It is evident that the silane concentration is similar for all samples, as also expected from the fact that the same molar concentration of organic species was used for the grafting procedure. This also suggests that steric hindrance problems between the organosilane chains are not significant during post-synthesis grafting.

TGA analysis of parent SBA-15 sample allowed estimating the concentration of surface silanol species by using Equation 1, where %OH = TGA weight loss between 200°C and 1100°C, due to the condensation of silanols group, 2 is the number of SiOH needed to form a water molecule by condensation, N<sub>A</sub> = Avogadro number (6.022\*10<sup>23</sup>), M.W.<sub>H<sub>2</sub>O</sub> = molecular weight of water (18.01 g/mol) and S.S.A is the Specific Surface Area of the parent sample, estimated by N<sub>2</sub> Physisorption Analysis.

$$\frac{\text{SiOH}}{\text{nm}^2} = \frac{\% \text{OH}}{100 - \% \text{OH}} * \frac{2 * N_A}{M.W._{H_2O} * S.S.A}$$

Equation 1: estimation of concentration of surface silanols.

The concentration of surface silanols calculated using Equation 1 is ca. 5.1 SiOH/nm<sup>2</sup>.

After the grafting procedure, assuming a complete reaction between the silane and the hydroxyl groups of the surface, ca. 3 SiOH/nm<sup>2</sup> are condensed for all samples during the amino-silane grafting and tridentate complexes are formed. This is an overestimation in that bidentate complexes may be also produced during the grafting procedure. Concerning one-pot prepared samples, the concentration of N species is similar to the grafted materials for all the samples.

The presence of organic species grafted on the SBA-15 surface silica was evaluated by FT-IR spectroscopy (figure 3).

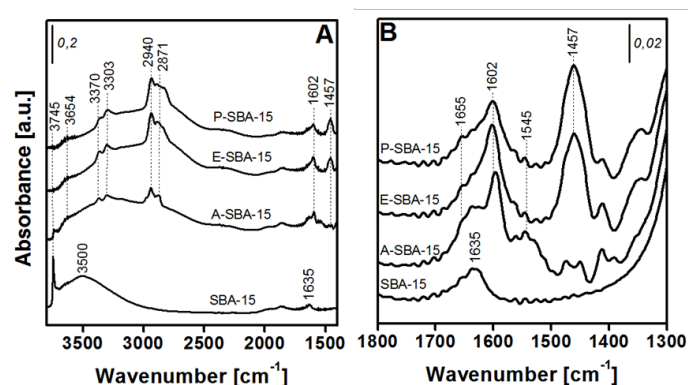


Fig. 3. Frame A: FT-IR spectra of bare SBA-15 and grafted samples. Frame B: enlargement of the FT-IR spectra in the 1800-1300 cm<sup>-1</sup> range. Spectra were recorded outgassing the samples at r.t. for 30 minutes.

In the high frequency range, the FT-IR spectrum of the pure SBA-15 silica sample (figure 3A) is characterized by the presence of two main bands located at 3745 cm<sup>-1</sup> (sharp) and at ca. 3500 cm<sup>-1</sup> (broad). The band at 3745 cm<sup>-1</sup> is due to the stretching mode of isolated silanol groups<sup>42</sup>, whereas the broad absorption at 3500 cm<sup>-1</sup> is due to the stretching mode of OH species interacting each other through H-bonding.<sup>21</sup>

As expected, after the grafting procedure the bands due to surface SiOH species appear strongly decreased in intensity (this is especially evident for E-SBA-15 and P-SBA-15 samples in which this band has an exceedingly low intensity) due to the fact that SiOH

species are involved in the grafting procedure. Interestingly, a residual amount of isolated SiOH species is still present on A-SBA-15 sample (figure 3A). Moreover, a broad band in the 3600–2500  $\text{cm}^{-1}$  range is visible in the IR spectrum of grafted samples. This band can be related to the formation of H-bonding interactions between surface silanols and amino groups of silane species introduced on the surface.

IR spectra of grafted samples are characterized by the presence of complex absorption in the 3500–2500  $\text{cm}^{-1}$  range, in which different components at 3370, 3303, 2940 and 2871  $\text{cm}^{-1}$  are visible. The absorptions at 3370 and 3303  $\text{cm}^{-1}$  are due to the asymmetric and symmetric stretching modes of  $\text{NH}_2$  groups, respectively, whereas the bands at 2940 and 2875  $\text{cm}^{-1}$  are assigned to the asymmetric and symmetric stretching modes of  $\text{CH}_2$  moieties of silane groups introduced onto the silica surface by the grafting procedure. The absorption bands in the low frequency region (figure 3B) are due to the scissoring mode of  $\text{NH}_2$  groups (band at 1600  $\text{cm}^{-1}$ ) and to the bending modes of  $\text{CH}_2$  groups (band located at 1457  $\text{cm}^{-1}$ )<sup>21</sup>. It can be noted that for A-SBA-15 sample, a fraction of  $\text{NH}_3^+$  species is also present, as attested by the bands at 1655 and 1545  $\text{cm}^{-1}$ .<sup>21</sup> The presence of the organic groups grafted on the SBA-15 silica surface was confirmed by the  $\text{T}^3$  ( $\text{Si}(\text{OSi})_3\text{C}$ ) and  $\text{T}^2$  ( $\text{Si}(\text{OSi})_2(\text{OCH}_3)\text{C}$ ) signals in  $^{29}\text{Si}$  MAS NMR spectra, and by well-defined resonances of carbon atoms of the organic chains in  $^{13}\text{C}$  CPMAS NMR spectra (see figures S3–S4 in the Supplementary Material).

Similar IR absorptions were also found for SBA-15 related samples prepared by one-pot procedure (figure S5 in the Supplementary Material). For these samples, it is interesting to note that the one-pot synthesis procedure, that is carried out at low pH, induces the protonation of the amino groups introduced on the sample surface, especially for A-SBA-15(OP) and E-SBA-15(OP) samples (as evidenced by FTIR analysis, figure S5 in the Supplementary Material). This is probably the main reason why these samples are less reactive towards  $\text{CO}_2$  with respect to post-synthesis grafted materials (vide infra). In the following part, in order to have additional insight on the role of the surface species in the  $\text{CO}_2$  capture process, only the data related to the more reactive grafted samples will be reported.

To account for all the protonic species in grafted systems, single pulse excitation  $^1\text{H}$  MAS NMR experiment were performed (figure 4). The direct acquisition of spectra allows the observation of both mobile and rigid components quantitatively as the line widths reflect and distinguish their presence. Pristine samples A-SBA-15 and P-SBA-15 show sharper narrow resonances at around 0.7 ppm due to methylene protons close to Si atoms. All the remaining methylene protons appear as a sharp peak at around 1.2 ppm. In addition, a peak at around 2 ppm due to surface silanols was also visible. On the contrary, no sharp resonances were detected for sample E-SBA-15. Here, all the EAPTS chains are in a confined environment where they experience reduced mobility. This is probably due to the inter- and/or intra-molecular interactions they are involved in. The former type of interaction is feasible with the silica surfaces at the interface through the involvement of non-covalent bindings by silanols and water, that is probably remaining

after the thermal treatment performed before analysis. Such a possibility will lead for the EAPTS side chains to adopt several conformations and result in heterogeneous broadening of resonance lines. However, very fast motions of the side chains in A-SBA-15 and P-SBA-15 averages out all  $^1\text{H}$ - $^1\text{H}$  dipolar interactions leading to narrow resonances. On the other hand, a very broad resonance peak centered at 5.7 ppm is visible in all the spectra and is associated with non-covalently interacting  $\text{NH}_2$  groups, physisorbed water remaining after the thermal activation treatment and hydrogen bonded silanols.

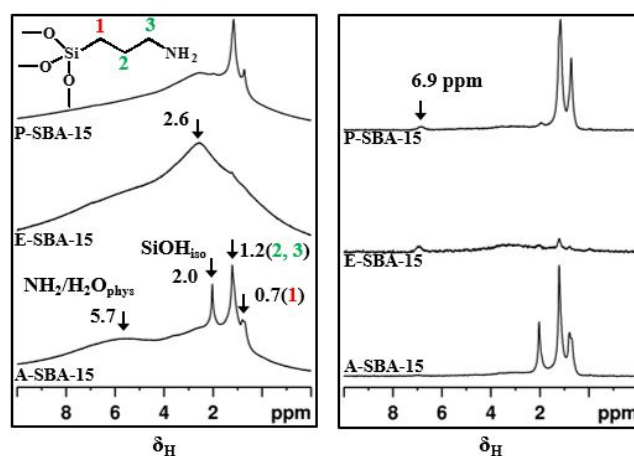


Fig. 4.  $^1\text{H}$  MAS NMR (left panel) and Hahn-echo NMR spectra (right panel) of hybrid SBA-15 samples prepared by grafting procedure.

Rotor synchronized Hahn-echo sequence was also applied to record the  $^1\text{H}$  NMR spectra with a  $\tau$  delay time of 6700  $\mu\text{s}$  (figure 4). The delay time was chosen as an optimized compromise between the signal decay owing to relaxation and the resolution gain owing to longer delay times. Using the rotor synchronized Hahn-echo sequence with long delay time, results in selective detection of mobile species. For this experiment, we rely on the differences in spin-spin relaxation of aliphatic chains, which are either mobile or rigid depending on their interactions with silica surface. Differentiation between rigid and mobile components can be accomplished in terms of the observed width of the resonance peaks. While the mobile components are detected as sharp narrow peaks, broader lines due to rigid components often are not resolved from the baseline.

Figure 4 shows the  $^1\text{H}$  NMR spectra recorded using Hahn-echo sequence of samples before  $^{13}\text{CO}_2$  adsorption. Samples A-SBA-15 and P-SBA-15 show sharper narrow resonances due to methylene protons of organic side chains. In addition, a peak at around 2 ppm was also visible which was due to isolated surface silanols. On the contrary, no sharp resonances were detected for sample E-SBA-15 and are associated with spatial confinement of EAPTS chains. This spectrum confirm that inter and/or intra-molecular interactions in pristine E-SBA-15 occur in/among the organic chains. One small peak at 6.9 ppm was also visible in all samples and was due to protonated amino groups. The  $^1\text{H}$  NMR experiments confirm that the EAPTS chains grafted on SBA-15 surface experience reduced



mobility compared to other samples. The possibility of molecular interactions among the grafted chains can be estimated by comparing the average free space around each amino-silane with a reasonable approximation of the molecular length. In Table 2, we report the average area of each silane domain on the surface (as the inverse of the organosilane density), and thus the average intermolecular distance (as the square root of this area); the chain lengths were obtained from the *ab initio* geometry optimizations described below.

The comparison shows that interactions are quite unlikely between APTS chains, whereas they could be observed between EAPTS and PAPTS. It has to be noted that these observations are only qualitative because they suppose a homogeneous distribution of organic chains.

Table 2. Distances between alkyl chain of silane in A-SBA-15, E-SBA-15 and P-SBA-15 silica samples.

Sample	Silane Density [n°chains/nm <sup>2</sup> ]	Intermolecular distance [Å]	Length of Silane <sup>a</sup> [Å]
A-SBA-15	0.9	10.5	5.3
E-SBA-15	1.1	9.5	7.1
P-SBA-15	1.0	10.0	8.9

<sup>a</sup> Length of the organosilane as determined by the geometry optimization described below.

The structure of the amino-silanes grafted on the silica surface was simulated theoretically with the method and the model clusters described above. First, one molecule of each organosilane (APTS, EAPTS and PAPTS) was added to cluster I, and the three adduct geometries were optimized. The final structures are shown in figure 5: in APTS-I model the relatively short chain and the rigidity of the tridentate organic-silica bond prevent the amino group to bend towards the surface, whereas the other, longer chains can lie down on the silica surface. One or two H-bonds were formed between silanols and amino groups in EAPTS-I and PAPTS-I, respectively: in the former case the bond appears stronger (O-N distance 2.5 Å in EAPTS-I, 2.7 and 2.8 Å in PAPTS-I); dispersion forces also provide a large contribution to the interaction energy between organic chains and surface (the weight of H-bond and dispersion interactions are of similar size, though the separation between them is somehow arbitrary).

To gain some insight on intermolecular interactions also, we optimized the structure of adducts with two molecules grafted on the larger cluster II, with the results reported in figure 6. The behavior of all the organosilane chains is similar to that observed for the smaller cluster: APTS tends to remain “perpendicular” to the surface, whereas both EAPTS and PAPTS lie closer to the silica surface. However, not all the PAPTS nitrogen atoms are H-bonded to the surface, since there are not enough silanol groups in a suitable position: this suggests that PAPTS motions could be less

hindered, even if this is just one of the possible conformations of the hybrid system. Note that the data in Tables 1 and 2 imply a density of grafted amino-silane of 0.9-1.1 molecules/nm<sup>2</sup> for all the systems: since the surface of the clusters, as said above, is around 2.5 and 4 nm<sup>2</sup>, respectively, the simulated densities with one molecule on cluster I and two on cluster II appear underestimated to some extent. Then two more adducts were optimized, grafting on cluster II three EAPTS or PAPTS molecules, respectively, since steric effects are expected to be more relevant for these systems than for the shorter APTS chains. In fact, as shown in figure 7, in both structures the third organosilane molecule is not able to approach the silica surface, and it remains almost perpendicular to the surface.

Note that in these models a homogeneous distribution of EAPTS and PAPTS on the surface was assumed, leading to distances between the organic chains of about 12 Å in the adducts with two molecules, and about 9 Å with three molecules. Some caution is required to interpret this result, since the use of a finite cluster model could be altered by border effects (in other words, the effective surface area could be smaller than 4 nm<sup>2</sup>, as obtained by the cluster side dimensions): nonetheless, these optimized adducts suggest that some organosilane chains, when the density is around 1 molecule/nm<sup>2</sup>, can be quite free to move far from the silica surface.

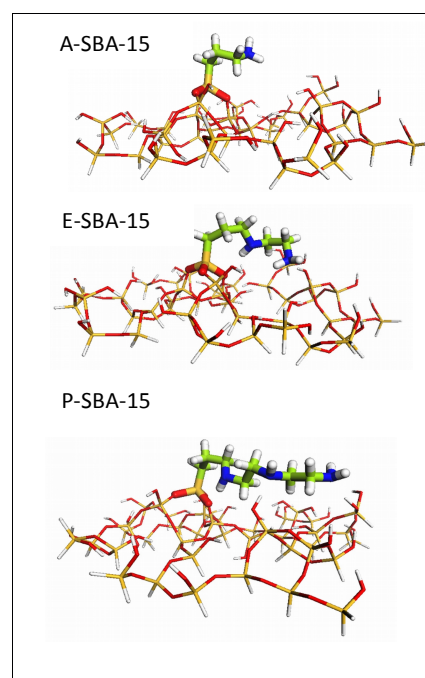


Fig. 5. Optimized structures of the adducts of APTS (a), EAPTS (b) and PAPTS (c) on silica model cluster I.

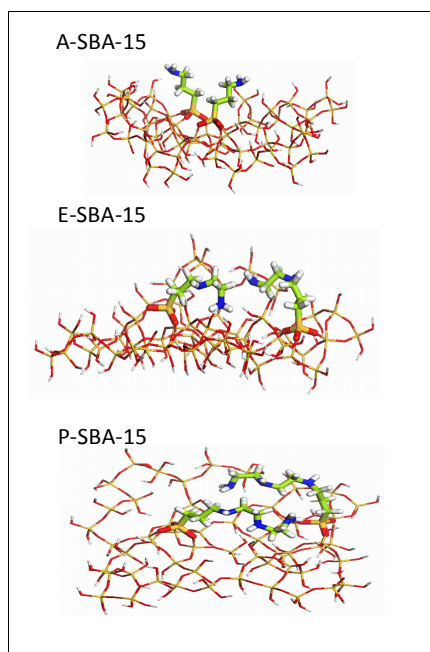


Fig. 6. Optimized structures of the adducts with two molecules of APTS (a), EAPTS (b) and PAPTS (c) on silica model cluster II.

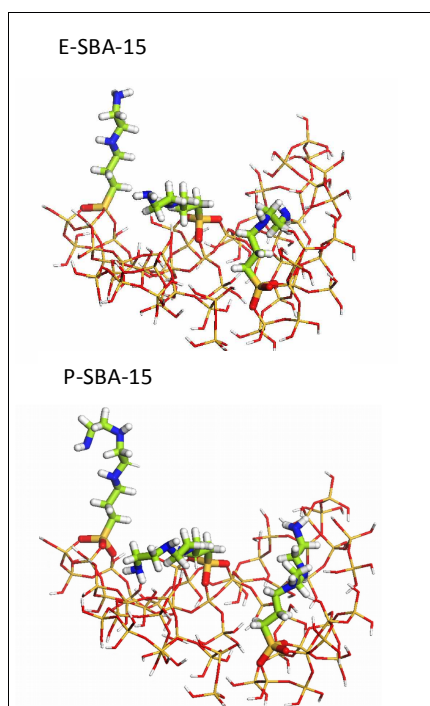


Fig. 7. Optimized geometry of the adducts with three EAPTS (a) and three PAPTS (b) molecules on silica cluster II.

### Study of reactivity between CO<sub>2</sub> and organo-modified SBA-15

Both infrared spectroscopy and solid-state NMR of adsorbed carbon dioxide were used to study the interactions between CO<sub>2</sub> and the basic group of the functionalized silica samples.

The IR spectra collected after admission of 60 mbar of CO<sub>2</sub> at beam temperature (BT) on samples prepared by both post-synthesis grafting and one-pot procedure are reported in figure 8.

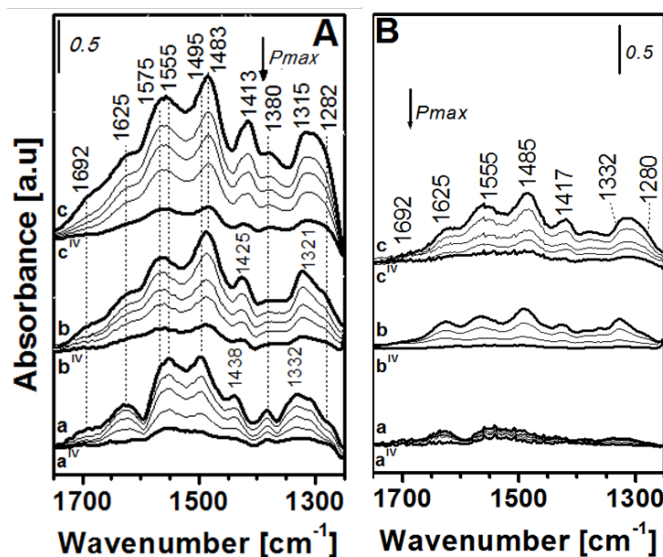


Fig. 8. FTIR spectra, in the 1750–1250 cm<sup>-1</sup> region, of CO<sub>2</sub> adsorbed ( $P_{max}$  = 60 mbar) at BT on grafted samples (frame A): A-SBA-15 (curves a-a<sup>IV</sup>), E-SBA-15 (curves b-b<sup>IV</sup>) and P-SBA-15 (curves c-c<sup>IV</sup>), and samples prepared by one-pot method (frame B): A-SBA-15(OP) (curves a-a<sup>IV</sup>), E-SBA-15(OP) (curves b-b<sup>IV</sup>) and P-SBA-15(OP) (curves c-c<sup>IV</sup>). The arrows indicate decreasing CO<sub>2</sub> pressure. Spectra are reported after subtraction of the spectrum of the bare sample (before CO<sub>2</sub> interaction) used as a background.

For the A-SBA-15 sample (figure 8, curve a), the admission of CO<sub>2</sub> leads to the formation of carbamate species as testified by bands located at 1555, 1495 and 1438 cm<sup>-1</sup> (see Table 3 for the assignment of the main bands). Moreover, peaks due to the presence of carbamic acid can be also found at 1692 and 1380 cm<sup>-1</sup>.<sup>1,43</sup> By decreasing progressively CO<sub>2</sub> pressure (figure 8, curves a<sup>I</sup>-a<sup>IV</sup>) bands related to carbamates and carbamic acid species progressively decrease in intensity thus indicating that part of the formed species are removed by outgassing procedure. From deconvolution of bands between 1410–1440 cm<sup>-1</sup>, chosen as representative of carbamate formation, and of the band at 1380 cm<sup>-1</sup>, representative of carbamic acid (data not shown for the sake of brevity), it has been observed that the intensity of the bands decrease in the same way both for carbamate and carbamic acid bands, thus indicating that the two species have approximately the same stability. Nevertheless, these species are in strong interaction with the sample surface, as witnessed by the fact that IR bands do not completely disappear upon outgassing at BT for 30 min (figure 8, curve a<sup>IV</sup>).

Concerning the E-SBA-15 and P-SBA-15 samples (figure 8, curves b-b<sup>IV</sup> and c-c<sup>IV</sup>), the admission of CO<sub>2</sub> also leads to the formation of carbamic acid and carbamate species. The deconvolution and integration of IR curves allowed us to estimate the ratio between the carbamates and carbamic acid formed upon CO<sub>2</sub> adsorption on the different samples. It was derived that the amount of

carbamates is similar for all samples whereas the quantity of carbamic acid increases passing from A-SBA-15 to P-SBA-15 sample. In addition, the presence of a shoulder located at ca.  $1575\text{ cm}^{-1}$  in E-SBA-15 and P-SBA-15 samples is due to the deformation of  $\text{NH}_2^+$  or to the combination of N-H deformation and C-N stretch vibrations in carbamates. This indicated that the samples containing more than one amino group in the chain react with  $\text{CO}_2$  to form an intramolecular carbamate ammonium salt.<sup>44</sup> The occurrence of intermolecular species is also indicated by the modification of the asymmetric bending of  $\text{NH}_3^+$  ( $1625\text{ cm}^{-1}$ ): the signal is almost resolved for the A-SBA-15 sample, whereas the absorption band become broader in the case of the E-SBA-15 and P-SBA-15 samples and this suggests the presence of residual  $\text{NH}_2^+$  groups.

Finally, shifts at lower frequency of both the symmetric stretching of  $\text{COO}^-$  group (from  $1438\text{ cm}^{-1}$  to  $1413\text{ cm}^{-1}$ ) and the  $\text{NCOO}^-$  skeletal vibration (from  $1332\text{ cm}^{-1}$  to  $1315\text{ cm}^{-1}$ ), probably due to the increasing of the length of organic chains, were observed.

As a matter of fact, in grafted samples the intensity of IR absorption increases along with the concentration of N atoms (i.e. on passing from the A-SBA-15 to the P-SBA-15 sample), thus suggesting that the higher the concentration of amine groups, the higher the reactivity towards  $\text{CO}_2$ .<sup>15</sup>

A similar behavior was observed for samples prepared by one-pot procedure. In this specific case, however, although the detected IR bands are in similar positions to those observed for grafted samples (thus suggesting the formation of the same species upon contact with  $\text{CO}_2$ ), the intensity of absorptions appeared significantly lower with respect to the analogous post-synthesis grafted samples. Although the two series of samples have a similar amount of N species (except the one-pot prepared samples with APTS species that has higher N content respect to the grafted analogous sample), the low reactivity associated to samples prepared via one-pot method can be explained considering that this procedure led to the formation of protonated amino groups, not suitable for reaction with  $\text{CO}_2$ .

The IR assignments of relevant peaks in the range are listed in Table 3.

Table 3: Assignments of the main FTIR bands formed upon  $\text{CO}_2$  adsorption on functionalized SBA-15 samples.

Wavenumber [ $\text{cm}^{-1}$ ]	Assignment	Ref.
1692	Stretching (C=O) of carbamic acid	45,46
1625	Asymmetric bending of $\text{NH}_2^+$ / $\text{NH}_3^+$	45, 47-50
1575	Deformation of $\text{NH}_2^+$ or combination of N-H deformation and C-N stretch vibrations in intermolecular carbamates	44
1555	Asymmetric stretching of C=O group of carbamate	50
1495-1483	Stretching of $\text{NHCOO}^-$ of Carbamate	45, 46, 48-53

1500-1485	Symmetric bending of $\text{NH}_2^+$ / $\text{NH}_3^+$	45, 47-51
1438-1413	Symmetric stretching of $\text{COO}^-$ group of carbamate	45, 47, 52
1380	bending of OH in carbamic acid	43, 52
1332-1315	$\text{NCOO}^-$ skeletal vibration	47
1282	Rocking of $\text{NH}_3^+$	45

Detailed information on the changes of the surface structures and the dynamics of the organic-functionalized SBA-15 samples prepared by post-synthesis after the introduction of  $^{13}\text{CO}_2$  were obtained by means of  $^{13}\text{C}$  CPMAS NMR. With respect to the pristine samples, no dramatic changes in chemical shifts of aliphatic carbons were observed for  $^{13}\text{CO}_2$  chemisorbed samples, however, broadening of all resonances are evident (Figure 9). Moreover, an additional resonance at 164 ppm was clearly visible in all the samples and was attributed to the presence of carbamate groups<sup>54</sup>. Moore et.al has studied  $\text{CO}_2$  adsorption on hyperbranched amine polymers grown from the mesoporous silica SBA-15 which exhibited mixture of chemisorption products, including carbamate, carbamic acid and bicarbonate moieties<sup>[55]</sup>. The resonance at 164 ppm lies near the chemical shift values expected for typical carbamic acid (160 ppm), bicarbonate (163 ppm) and carbamate (164 ppm) species. The full width at half-maximum (fwhm), around 4 ppm, of this resonance is larger than the chemical shift difference ( $\sim 3\text{ ppm}$ ) between these products. Therefore, the presence of carbamic acid and bicarbonate moieties cannot be excluded from the systems studied here. On the other hand, Moore et al. have observed mixture of chemisorption products due to the presence of primary, secondary, and tertiary amines, which enables multiple reactions through multiple pathways. Furthermore, they have observed that upon evacuation more loosely bound chemisorbed  $\text{CO}_2$  products were desorbed. In our study mostly firmly bound carbamate species are found on the surface of organically modified SBA-15, probably because of the absence of tertiary amines. Furthermore,  $^{13}\text{C}$  CPMAS NMR data revealed the presence of an additional fraction of physisorbed  $^{13}\text{CO}_2$ , especially in the case of P-SBA-15. Previous studies have demonstrated the formation of carbamate group as well as the physisorption of  $^{13}\text{CO}_2$  in amine-modified porous materials<sup>50</sup>. The intensity of the signal due to the carbamate specie increases along with the concentration of N atoms. These results, in line with those obtained by FTIR, suggested that the amount of amino groups influence the reactivity with the  $^{13}\text{CO}_2$ .

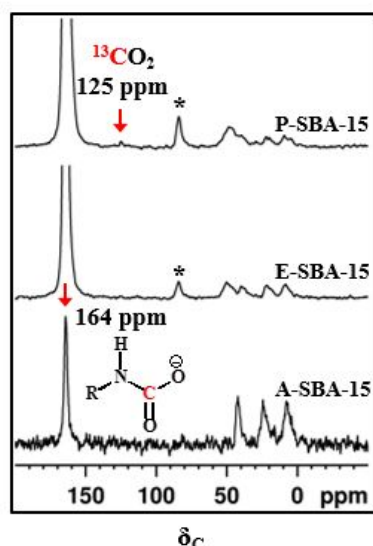


Fig. 9.  $^{13}\text{C}$  CPMAS NMR spectra of  $^{13}\text{CO}_2$  adsorbed on grafted SBA-15 samples. A cross polarization contact time of 2 ms and a MAS rate of 10 kHz was used in all the experiments. \* Denote spinning side-bands.

Figure 10 shows the  $^1\text{H}$  MAS NMR and Hahn-echo NMR spectra of samples after  $^{13}\text{CO}_2$  adsorption. A reduction in mobile components was clearly visible in sample P-SBA-15 after the  $^{13}\text{CO}_2$  adsorption. However, the peak due to surface silanols was missing from sample A-SBA-15 after  $^{13}\text{CO}_2$  adsorption although the behavior of side chains was similar as before the adsorption. An increase in the amount of protonated amino groups was clearly visible in all the three samples. Before the introduction of  $^{13}\text{CO}_2$ , A-SBA-15 and P-SBA-15 samples showed similar amount of mobile and rigid components. On the contrary, only rigid components were visible in sample E-SBA-15 as confirmed by the absence of sharp peaks in the high resolution Hahn-echo NMR spectra presented here. However, an increase in the rigid part was clearly observed for all the samples after their exposure to  $^{13}\text{CO}_2$ . In conclusion, the behavior of different chains on the interface is diverse as they are capable of non-covalent interactions. Such interactions will lead to a distribution of chain conformations at the interface, which are reflected as broad resonance lines. Nevertheless, a significant fraction of these chains in samples A-SBA-15 and P-SBA-15 are capable of isotropic motions, which are revealed as sharp peaks. The conversion of amino group into carbamate species upon  $^{13}\text{CO}_2$  introduction does not influence the molecular dynamics of side chains at the interface.

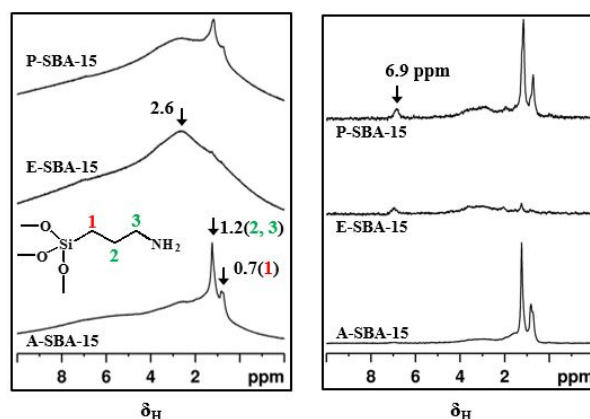


Fig. 10.  $^1\text{H}$  MAS NMR and Hahn-echo NMR spectra of samples after  $^{13}\text{CO}_2$  adsorption on SBA-15 grafted samples.

### Study of the $\text{CO}_2$ capture capacity

The isotherms relative to the adsorption at  $30^\circ\text{C}$  of carbon dioxide on the three amino-functionalized SBA-15 are reported, as a function of the  $\text{CO}_2$  equilibrium pressure (see full symbol curves) in Figure 11 and S6 (these latter isotherms were calculated at very low equilibrium pressures). The  $\text{CO}_2$  uptake capacity of the three samples, at pressures lower than 150 mbar, follows the trend reported in the FT-IR adsorption experiments, i.e. P-SBA-15>E-SBA-15>A-SBA-15. Independently from the sample, the three quantitative isotherms indicate a specific adsorption pathway in which it is possible to distinguish the initial adsorption of carbon dioxide on the more reactive amine sites at low pressures (with the formation of carbamate species),<sup>56,57</sup> followed by a filling of the available pore volume at higher pressure. In particular, both systems grafted with alkylamine chains containing more than one amino group (E-SBA-15 and P-SBA-15) exhibit isotherms with a steep increase (more evident for the P-SBA-15 sample) for pressure lower than 10 mbar and a gradual increase from 5 to 500 mbar. Still, the quantitative isotherms of the systems containing two or three amino groups change behaviour at higher  $\text{CO}_2$  pressures. For  $p > 300$  mbar, in fact, the E-SBA-15 isotherm is still clearly growing with respect to the P-SBA-15 isotherm that is slowly approaching to its plateau. The material functionalized with the plain amino-propyl group (A-SBA-15) exhibits a peculiar isotherm with an evident step between 60 and 100 mbar and an appreciably lower overall adsorption capacity per gram of sample, especially at low equilibrium pressures. The definitely lower amount of adsorbed  $\text{CO}_2$  in the case of the A-SBA-15 is related to the different adsorption way of this molecule in presence of a shorter alkylamine chain. In this case, in fact, the formation and following stabilization of the carbamate species occurs between two adjacent amine chains (intermolecular  $\text{CO}_2$  adsorption): only the amino groups located at the right distance are effective adsorption sites for carbon dioxide.<sup>56</sup> This problem is exceeded in E-SBA-15 and P-SBA-15 in which the adsorption of carbon dioxide proceeds via the formation of intramolecular carbamate species<sup>57</sup>. In this last case all the alkylamine chains are potentially able to react with one  $\text{CO}_2$  molecule forming and stabilizing an alkylammonium carbamate.



The intramolecular cooperative adsorption with the formation of an alkylammonium carbamate occurs between the  $\text{NH}_2$  and the  $\text{NH}$  moieties of the alkylamine chain. For this reason, even if the P-SBA-15 sample contains two  $\text{NH}$  groups the capture of a second  $\text{CO}_2$  molecule is not possible and, therefore, the overall  $\text{CO}_2$  adsorption capacity is only slightly higher in the case of P-SBA-15. On the contrary, as mentioned above, at low pressure, the P-SBA-15 is able to adsorb a definitely higher amount of carbon dioxide. These data suggest that, probably, the intramolecular species are more efficiently formed by two amines separated by more than two atoms, i.e. when the amine chain is more flexible (*vide supra the computational part*).

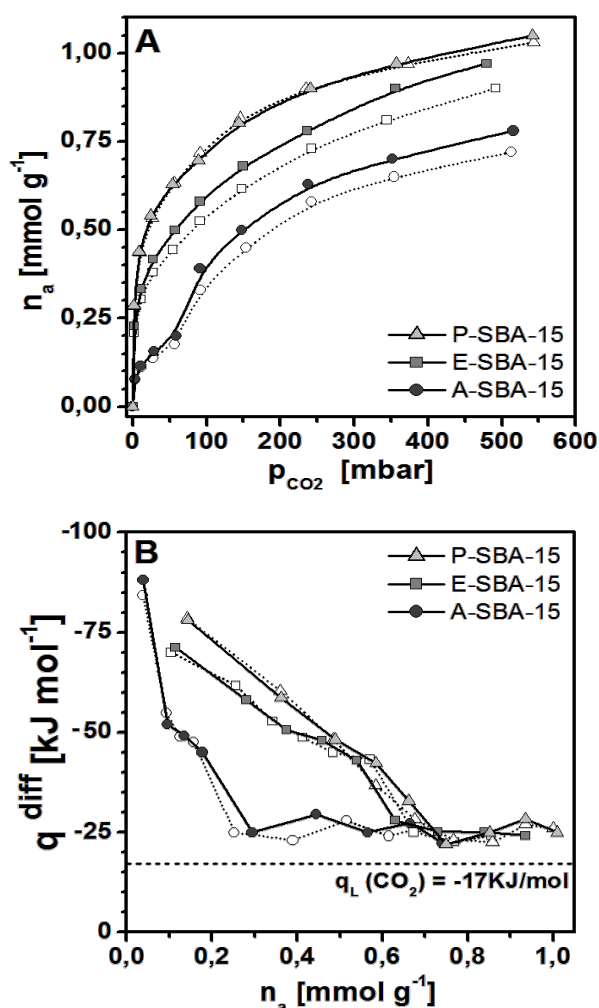


Fig. 11. Frame A) Quantitative isotherms related to the adsorption at 30°C of  $\text{CO}_2$  on A-SBA-15 (circle), E-SBA-15 (squares) and P-SBA-15 (triangle) samples. Frame B) Differential molar adsorption heats related to the adsorption of  $\text{CO}_2$  on grafted SBA-15 samples. The dashed horizontal line represents the standard molar enthalpy of liquefaction of  $\text{CO}_2$  at 298K. Solid symbols represent the primary adsorption runs and empty symbols the secondary adsorption ones.

Moreover, the presence of the step in the isotherm of the A-SBA-15 sample can probably derive from the possibility of this material to interact with  $\text{CO}_2$  in two different ways: (i) through the cooperation of an amine chain with a surface residual silanol group (as

demonstrated by the FT-IR analysis, the residual amount of isolated  $\text{SiOH}$  species is clearly higher in the case of the A-SBA-15) forming a carbamic acid species stabilized by the interaction with a surface  $\text{OH}$  group: (ii) through the formation of a carbamate species between two adjacent amine chains. The intermolecular amine-amine adsorption is probably favoured at higher equilibrium pressures. This phenomenon could explain the presence of the step at around 60 mbar.

Also E-SBA-15 and P-SBA-15 can interact with  $\text{CO}_2$  in two different ways: (i) through the cooperation of an amine chain with a surface residual silanol group with the formation of carbamic acid or (ii) through the formation of intramolecular carbamate species. However, their  $\text{CO}_2$  adsorption isotherms do not exhibit the step at low equilibrium pressures (as A-SBA-15), probably because these two interaction ways are both favoured independently from the  $\text{CO}_2$  pressure.

Moreover, taking into account that from IR data it was derived that the quantity of carbamic acid species increases passing from A-SBA-15 to P-SBA-15 sample, it is clear that, despite the lower amount of residual isolated  $\text{SiOH}$  species of E-SBA-15 and P-SBA-15 with respect to A-SBA-15, the simultaneous interaction of  $\text{CO}_2$  with an amine and a residual surface  $\text{OH}$  group (with the formation of carbamic acid) seems to be favoured due to the higher mobility of longer amine chains that allows their approach also to far  $\text{OH}$  species during the cooperative interaction with  $\text{CO}_2$ . In particular, the higher is the length of the grafted alkylamine chain, the higher is the amount of formed carbamic acid.

Comparing our results to those reported by Yoo et al. [15] for similar sorbents (i.e. SBA-15 grafted with APTS, EAPTS and PAPTS), but containing lower amount of organosilane, we can see a significant effect of the silane density. In the work cited, in which the silane concentration is deliberately low (0.45 mmol/g), the  $\text{CO}_2$  adsorption capacity values are 0.05, 0.08 and 0.125 mmol/g, respectively for A-SBA-15, E-SBA-15 and P-SBA-15 at a pressure of 60 mbar. However, in our study, in which the silane concentration is around 1 mmol/g (that is around the double that in the cited work), the  $\text{CO}_2$  adsorption capacity values at the same pressure are significantly increased for each sample: 0.20, 0.50 and 0.64 mmol/g, respectively, for A-SBA-15, E-SBA-15 and P-SBA-15 (i.e. more than four times of the values reported by Yoo). These values suggested that the high amine loading on the SBA-15 surface is effective to increase the adsorption capability towards  $\text{CO}_2$  probably because of the propinquity of reactive species on the surface. The fact that this effect is more pronounced for E-SBA-15 and P-SBA-15 samples could be related to a favourable arrangement of organic chains on the silica surface at high silane loading. The comparison between primary (full symbols) and secondary (empty symbols) adsorption isotherms in figure 11(A) highlights an almost total reversibility of the adsorbed  $\text{CO}_2$  in the case of A-SBA-15 and E-SBA-15, and a total reversibility in the case of P-SBA-15. These last results are not in perfect agreement with the data reported in the FT-IR section probably in relation to the short outgassing time employed upon FTIR  $\text{CO}_2$  adsorption respect to calorimetric analysis. Differential molar adsorption heats of the various samples are reported in

Figure 11(B) and S6(B) (for very low coverages) as a function of the adsorbed amounts. These values are in agreement with the data reported in the literature for similar systems<sup>58,59</sup>. For what concerns the A-SBA-15 material, the adsorption enthalpy starts at very high values (higher than  $-90 \text{ kJ mol}^{-1}$ ; zero-coverage differential heat of adsorption  $q_0 \sim -120 \text{ kJ mol}^{-1}$ ) and this suggests the presence of a small fraction of extremely energetic sites, i.e. the strongest in terms of energy of interaction and, therefore, active in the earliest stages of the adsorption process (in this specific case, they are probably, couples of amine chains with a particularly favourable position for the formation of the intermolecular carbamate species). Then, the adsorption heat decreases fast with increasing carbon dioxide loading to about  $-25 \text{ kJ mol}^{-1}$ . The enthalpy values in the  $-90 - -45 \text{ kJ mol}^{-1}$  range can be attributed to the strong interaction between the carbon dioxide molecules, the adjacent amine groups and the residual surface silanols forming intermolecular carbamate species and carbamic acid species. Then, once all available amine and SiOH groups (i.e. located at the right distance for the effective cooperative adsorption of  $\text{CO}_2$ ) have interacted with  $\text{CO}_2$ , the gas adsorbs on less reactive surface sites (residual surface silanols). A very similar trend can be observed for the other two samples (E-SBA-15 and P-SBA-15). In this case, however, the initial adsorption enthalpy starts at lower values (around  $-80 \text{ kJ mol}^{-1}$ ; zero-coverage differential heat of adsorption  $q_0 \sim -100 \text{ kJ mol}^{-1}$ ) and proceeds declining slowly to  $\sim -45 \text{ kJ mol}^{-1}$ . The definitely lower values of enthalpy at zero coverage, observed for these two samples with respect to the A-SBA-15, can be explained considering that, as demonstrated by the computational calculations, the longer amine chains (EAPTS and PAPTS) can lie down on the silica surface and form H-bonds with residual surface silanols. Before the interaction with the  $\text{CO}_2$  molecules, these H-bonds have to be broken leading to a decrease of the first values of adsorption heat for these samples. The enthalpy values in the  $-80 - -50 \text{ kJ mol}^{-1}$  range can be associated with the  $\text{CO}_2$  adsorbed via intramolecular interactions.<sup>57,58</sup> Then, when all the amine groups have interacted with  $\text{CO}_2$  the adsorption enthalpy decreases until to  $-25 \text{ kJ mol}^{-1}$ , tending to the asymptotic value of carbon dioxide molar liquefaction enthalpy ( $-17 \text{ kJ mol}^{-1}$ ) which is characteristic of the uptake phase dominated by metastable liquid-like physical adsorption.

The chemisorbed  $\text{CO}_2$  amount can be easily derived from Figure 11(B), considering the amount of adsorbed  $\text{CO}_2$  corresponding to the enthalpy values (in the range between  $-90$  and  $-40 \text{ kJ/mol}$ ) associated with the  $\text{CO}_2$  adsorption via intermolecular or intramolecular interactions with the alkylamine chains, thus avoiding the contribution of physisorbed  $\text{CO}_2$ . The chemisorbed amount on A-SBA-15, E-SBA-15 and P-SBA-15 is ca. 0.2, 0.6 and 0.7 mmol/g respectively, apparently much lower with respect to the amino groups content (ca. 1, 2.6 and 3.5 mmol/g for A-SBA-15, E-SBA-15 and P-SBA-15 respectively). For what concerns the A-SBA-15 sample, the formation and following stabilization of the carbamate species occurs between two adjacent amine chains and only two amino groups located at the right distance are effective adsorption sites for carbon dioxide. This type of interaction is responsible for

the low  $\text{CO}_2$  chemisorbed amount ( $\sim 0.2 \text{ mmol/g}$ ) of this material with respect to its content of amino groups (1 mmol/g). In fact, two different amino groups are necessary to form the carbamate species and, therefore, the amount of  $\text{CO}_2$  that could be actually chemisorbed by this material is no higher than 0.5 mmol/g and, moreover, the number of amine chains located at the right distance to allow the formation of the carbamate species can be restricted. On the other hand, in the case of E-SBA-15 and P-SBA-15 the adsorption of carbon dioxide proceeds via the formation of intramolecular carbamate species. Potentially, all the alkylamine chains can interact with one  $\text{CO}_2$  molecule by means of a  $\text{NH}_2$  group and a  $\text{NH}$  moiety at the same time: in the case of E-SBA-15, containing  $\sim 2.6 \text{ mmol/g}$  of amino groups, the potential chemisorbed  $\text{CO}_2$  uptake can be not higher than  $\sim 1.3 \text{ mmol/g}$ , whereas for P-SBA-15 (with an amino groups content of  $\sim 3.5 \text{ mmol/g}$  and containing one  $\text{NH}_2$  group and two  $\text{NH}$  moieties for each chain) one third of the amino groups does not take part to the intramolecular cooperative adsorption and, as a consequence, the potential amount of  $\text{CO}_2$  that can be adsorbed by the amine chains is not higher than  $\sim 1.2 \text{ mmol/g}$ . However, for E-SBA-15 and P-SBA-15 the actual chemisorbed  $\text{CO}_2$  uptake is  $\sim 0.6$  and  $\sim 0.7 \text{ mmol/g}$  respectively, i.e. definitely lower than 1.3 and 1.2 mmol/g. As demonstrated by the computational calculations, the longer amine chains (EAPTS and PAPTS) lie down on the silica surface and form H-bonds with the residual surface silanols that have to be broken before the interaction with the  $\text{CO}_2$  molecules. Probably, this circumstance may not always occur, so explaining the lower amount of chemisorbed  $\text{CO}_2$  with respect to the real amino groups content of these two materials.

### Study of $\text{CO}_2$ capture capacity in post combustion conditions

The adsorption of  $\text{CO}_2$  was also monitored using the ZLC method to determine quantitatively the  $\text{CO}_2$  uptake. This is an innovative and advantageous screening method for amino-grafted silica adsorbents, because it requires very small amount of samples (10–15 mg) and short experimental time (about 1 hour per test).

Figure 12A shows an example of the ZLC desorption curve for the P-SBA-15 sample. The data are plotted as dimensionless concentration,  $C/C_0$  ( $C_0 = \text{CO}_2$  concentration in the gas phase at equilibrium), vs. the volume of gas eluted  $Ft$  ( $F = \text{inlet flowrate of the carrier, He}$ ). The plot includes the blank curves, i.e. the response of the system when no sample is loaded. Based on the mass balance of the column the difference between the area under the desorption curve of the sample and the blank is proportional to the amount adsorbed: the  $\text{CO}_2$  uptake can be then calculated by integration.<sup>23,60</sup>

By normalizing the  $Ft$  plot by the mass of the sample,  $M$ , the ranking of the  $\text{CO}_2$  uptake for each SBA-15 sample can be visually compared, as shown in figure 12B. Table 4 summaries the capacities calculated for the ZLC desorption curves for the different samples (note that the ZLC experiments were carried out 0.1 bar partial pressure of  $\text{CO}_2$  and  $35^\circ\text{C}$ ). The sequence of the  $\text{CO}_2$  capacities is



excellent agreement with the volumetric measurements (Figure 11), with P-SBA-15 > E-SBA-15 > A-SBA-15.

It is worth noting that the ZLC method measures the amount desorbed from the sample. For a purely physisorption process this is the same as the amount originally adsorbed in the sample. In this case it seems very likely that a portion of the amount adsorbed is chemically bound to the amine groups, therefore irreversibly adsorbed during the time of the experiment. Temperature programmed desorption (TPD) was carried out on some of the samples, but the signal related to the amount desorbed at high temperature was too close to the detector baseline to be accurately quantified. This, together with the difference in temperature between the two experiments, explains the small discrepancy with the adsorbed amount measured at 25°C in the volumetric system. The amount adsorbed for the samples is particularly low at these conditions and as a result the experimental ZLC curves are too close to the blank curves. This unfortunately prevents any further analysis on the equilibrium and the kinetics of adsorption.

For carbon capture applications fast adsorption cycles (seconds or minutes) are desirable to achieve high productivity, it is then important to evaluate the performance of novel adsorbents under conditions representative of the real application. For this reason, in this study each ZLC test was carried out for no more than 1 hour in total (adsorption and desorption).

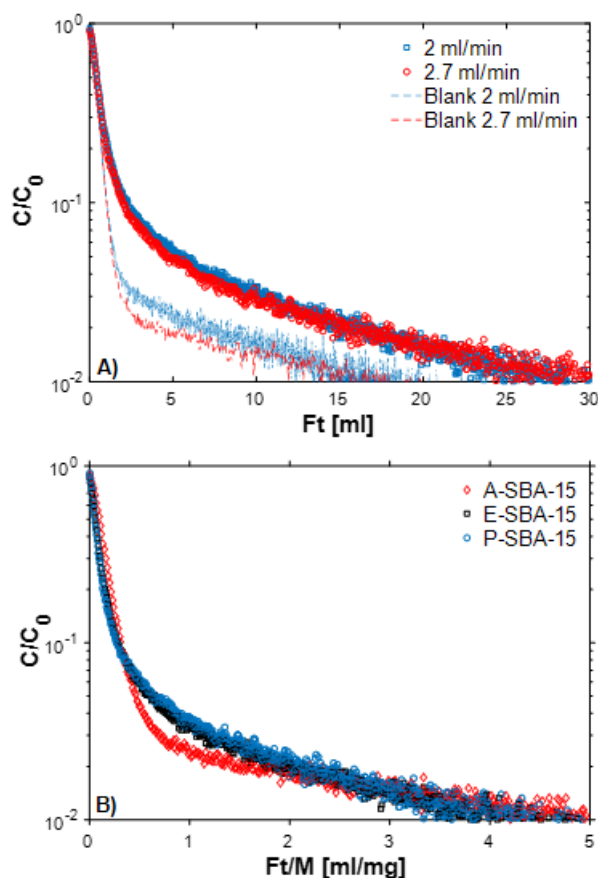


Fig. 12. Section (A) – ZLC desorption curves for P-SBA-15 sample and blank curves at 2 and 2.7 ml/min flow rates. Section (B) – ZLC desorption curves for A-SBA-15, E-SBA-15 and P-SBA-15 samples (CO<sub>2</sub> partial pressure: 0.1 bar, flow rate: 2 ml/min, T: 35°C).

Table 4. Comparison between ZLC and calorimetric results for CO<sub>2</sub> adsorption at low pressure.

Sample	ZLC*			Calorimetric measurements**
	CO <sub>2</sub> [mmol g <sup>-1</sup> ]	CO <sub>2</sub> [mg g <sup>-1</sup> ]	CO <sub>2</sub> /N ratio	CO <sub>2</sub> [mmol g <sup>-1</sup> ]
SBA-15	0.16	6.2	-	-
A-SBA-15	0.23	9.2	0.20	0.31
E-SBA-15	0.39	16.7	0.15	0.51
P-SBA-15	0.51	22.4	0.15	0.68

\* ZLC working conditions: i) Total pressure: 1 bar; ii) CO<sub>2</sub> partial pressure: 0.1 bar; total pressure: 1 bar iii) temperature 35°C; iv) dosage gas composition 90% He–10% CO<sub>2</sub>. \*\*Calorimetric conditions: i) CO<sub>2</sub> partial pressure: 0.1 bar; ii) temperature 30 °C.

## Conclusions

The adsorption properties of SBA-15, both prepared via one-pot and grafted post synthesis with APTS, EAPTS and PAPTS, were studied with a multidisciplinary approach. Both infrared spectroscopy and solid-state NMR of adsorbed carbon dioxide provided information on the interactions between CO<sub>2</sub> and the basic group of the functionalized silica samples. These techniques confirmed the formation of carbamate species, as a result of chemical interactions between basic amino groups and the carbon dioxide. Both FT-IR and SS-NMR spectroscopies suggested that increasing the number of amino groups in the chain, i.e. passing from A-SBA-15 to P-SBA-15 sample, increase also the reactivity toward CO<sub>2</sub>. Nevertheless, samples prepared via post-synthesis grafting procedure, are more reactive towards CO<sub>2</sub> with respect one-pot synthesized ones due to the fact that for these last samples the preparation step in acid conditions led to the protonation of amino groups.

A deeper analysis of the most reactive post-grafted samples was carried out. <sup>1</sup>H Hahn echo MAS NMR spectroscopy suggested that A-SBA-15 and P-SBA-15 samples display similar amount of mobile and rigid components, while E-SBA-15 shows only rigid components. This behavior agrees with the results of ab initio modeling: the optimized adducts of the three organosilanes on some silica cluster models show that APTS chain interacts loosely with the surface, as well as PAPTS when the density of the grafted molecules is high enough. In addition, after the introduction of <sup>13</sup>CO<sub>2</sub>, an increase in the rigid part was clearly observed for all the samples.

Finally, for the first time, the amount of adsorbed carbon dioxide on SBA-15 grafted with amino-silanes were estimated comparing two

different quantitative techniques: a classical microcalorimetric analysis and the Zero- Length Column chromatography. In particular, the obtained values of the CO<sub>2</sub> adsorption capacity by means of microcalorimetry are 0.31, 0.51 and 0.68 mol/kg, respectively for A-SBA-15, E-SBA-15 and P-SBA-15, while the CO<sub>2</sub> adsorption capacity values obtained with ZLC are 0.21, 0.44 and 0.53 mol/kg, respectively for A-SBA-15, E-SBA-15 and P-SBA-15.

## Acknowledgements

The financial support of the PRIN Project n° 2010A2FSS9 entitled: "Mechanisms of CO<sub>2</sub> activation for the design of new materials for energy and resource efficiency" is gratefully acknowledged.

## Notes and references

- 1 B. Li, Y. Duan, D. Luebke, B. Morreale, *Applied Energy*, 2013, **102**, 1439-1447.
- 2 S.Y. Lee, S.Y. Park, *Journal of Industrial and Engineering Chemistry*, 2015, **23**, 1-11.
- 3 Q. Wang, L. Luo, Z. Zhong, A. Borgna, *Energy Environ. Sci.*, 2011, **4**, 42-55.
- 4 J. Wang, L. Huang, R. Yang, Z. Zhang, J. Wu, Y. Gao, Q. Wang, D.O'Hareb, Z. Zhong, *Energy Environ. Sci.*, 2014, **7**, 3478-3518.
- 5 A. Samanta, A. Zhao, G.K.H. Shimizu, P. Sarkar, P. Gupta, *Ind. Eng. Chem. Res.*, 2012, **51**, 1438-1463. (13)
- 6 J. Tang, J. Liu, N.L. Torad, T. Kimura, Y. Yamauchi, *Nanotoday*, 2014, **9**, 3, 305-323.
- 7 K. C. Wu, Y. Yamauchi, *J. Mater. Chem.*, 2012, **22**, 1251-1256.
- 8 V. Malgras, H. Ataee-Esfahani, H. Wang, B. Jiang, C. Li, K. C.-W. Wu, J. H. Kim, Y. Yamauchi, *Adv. Mater.*, 2016, **28**, 6, 993-1010.
- 9 V. Malgras, Q. Ji, Y. Kamachi T. Mori, F.-K. Shieh, K.C.W. Wu, K. Ariga, Y. Yamauchi, *Bull Chem Soc Jpn*, 2015, **88**, 1171-1200.
- 10 C.H. Yu, C.H. Huang, C.S. Tan, *Aerosol and Air Quality Research*, 2012, **12**, 745-769.
- 11 C. Chen, J. Kim, W.S. Ahn, *Korean J. Chem. Eng.*, 2014, **31**, 1919-1934.
- 12 M. Caplow, *J. Am. Chem. Soc.*, 1968, **90**, 6795-6803.
- 13 B. Dutcher, M. Fan, A.G. Russell, *Appl. Mater. Interfaces*, 2015, **7**, 2137-2148.
- 14 A. Sayari, A. Heydari-Gorji, Y. Yang, *J. Am. Chem. Soc.*, 2012, **134**, 13834-13842.
- 15 C.Y. Yoo, L.C. Lee, C.W. Jones, *Langmuir*, 2015, **31**, 13350-13360.
- 16 V. Zelenák, M. Badanicová, D. Halamová, J. Cejka, A. Zukal, N. Murafa, G. Goerigk, *Chem. Eng. J.*, 2008, **144**, 336-347.
- 17 X. Yan, L. Zhang, Y. Zhang, Y. Yang, Z. Yan, *Ind. Eng. Chem. Res.*, 2011, **50**, 3220-3226.
- 18 F.Y. Chang, K.J. Chao, H.H. Cheng, C.S. Tan, *Sep. Purif. Technol.*, 2009, **70**, 87-95.
- 19 Y. Li, X. Wen, L. Li, F. Wang, N. Zhao, F. Xiao, W. Wei, Y. Sun, *J. Sol-Gel Sci. Technol.*, 2013, **66**, 353-362.
- 20 D. Zhao, Q. Huo, J. Feng, B.F. Chmelka, G.D. Stucky, *J. Am. Chem. Soc.*, 1998, **120**, 6024-6030.
- 21 L. Etgar, G. Schuchardt, D. Costenaro, F. Carniato, C. Bisio, S.M. Zakeeruddin, M.K. Nazeeruddin, L. Marchese, M. Graetzel, *J. Mater. Chem. A*, 2013, **1**, 10142-10147. (39)
- 22 S. Hao, H. Chang, Q. Xiao, Y. Zhong, W. Zhu, *J. Phys. Chem. C*, 2011, **115**, 12873-12882.
- 23 D. Massiot, F. Fayon, M. Capron, I. King, S. Le Calve, B. Alonso, J.O. Durand, B. Bujoli, Z. Gan, G. Hoatson, *Magn. Reson. Chem.*, 2002, **40**, 70-75.
- 24 M. Eic, D.M. Ruthven, *Zeolites*, 1988, **8**, 40-45.
- 25 X. Hu, S. Brandani, A.I. Benin, R.R. Willis, *Industrial & Engineering Chemistry Research*, 2015, **54**, 6772-6780.
- 26 J.A.A. Gibson, E. Mangano, E. Shiko, A.G. Greenaway, A.V. Gromov, M. Lozinska, D. Friedrich, E.E.B. Campbell, P.A. Wright, S. Brandani, *Industrial & Engineering Chemistry Research*, 2016, **55**, 3840-3851.
- 27 S. Brandani, D.M. Ruthven, *Adsorption*, 1996, **2**, 133 - 143.
- 28 V. Bolis, C. Busco, V. Aina, C. Morterra, P. Ugliengo, *J. Phys. Chem. C*, 2008, **112**(43), 16879-16892.
- 29 A.D. Becke, *Phys. Rev. B*, 1988, **38**, 3098- 3105.
- 30 C. Lee, W. Yang, R.G. Parr, *Phys. Rev. B*, 1988, **37**, 785-791.
- 31 A.D. Becke, *J. Chem. Phys.*, 1993, **98**, 1372-1381.
- 32 T.H. Dunning, *J. Chem. Phys.*, 1989, **90**, 1007-1010.
- 33 R.A. Kendall, T.H. Dunning, R.J. Harrison, *J. Chem. Phys.*, 1992, **96**, 6796-6801.
- 34 P.J. Hay, W.R. Wadt, *J. Chem. Phys.*, 1985, **82**, 270-279.
- 35 T. Schwabe, S. Grimme, *Phys. Chem. Chem. Phys.*, 2006, **8**, 4398-4404.
- 36 P. Ugliengo, M. Sodupe, F. Musso, I. J. Bush, R. Orlando, R. Dovesi, *Adv. Mater.*, 2008, **20**, 4579-4583.
- 37 J.M.R. Gallo, C. Bisio, G. Gatti, L. Marchese, H.O. Pastore, *Langmuir*, 2010, **26**, 5791-5800.
- 38 S. Lowell, J.E. Shields, M.A. Thomas, M. Thommes, *Kluwer Academic Publishers*, 2004.
- 39 F. Hoffmann, M. Cornelius, J. Morell, M. Fröba, *Angew. Chem. Int. Ed.*, 2006, **45**, 3216-3225.
- 40 M. Thommes, K. Kaneko, A.V. Neimark, J.P. Olivier, F. Rodriguez-Reinoso, J. Rouquerol, K.S.W. Sing, *Pure Appl. Chem.*, 2015, **87**(9-10), 1051-1069.
- 41 M. Kruk, M. Jaroniec, *Chem. Mater.*, 2000, **12**, 1961-1968.
- 42 F. Cucinotta, F. Carniato, G. Paul, S. Bracco, C. Bisio, S. Caldarelli, L. Marchese, *Chem. Mater.*, 2011, **23** (11), 2803-2809.
- 43 M.W. Hahn, M. Steib, A. Jentys, J.A. Lercher, *J. Phys. Chem. C*, 2015, **119**, 4126-4135.
- 44 Z.F. Tran, D. Busche, B. Fryxell, L. Addleman, R. Zemanian, T. Aardahl, L. Christopher, *Ind. Eng. Chem. Res.*, 2005, **44**, 3099-3105.
- 45 G. Socrates, JOHN WILEY & SONS, LTD, 2001.
- 46 C. Knofel, C. Martin, V. Hornebecq, P.L. Llewellyn, *J. Phys. Chem. C*, 2009, **113**, 21726-21734.
- 47 X. Wang, W. Schwartz, J.C. Clark, X. Ma, S.H. Overbury, X. Xu, C. Song, *J. Phys. Chem. C*, 2009, **113**, 7260-7268.
- 48 H.Y. Huang, R.T. Yang, D. Chinn, C.L. Munson, *Ind. Eng. Chem. Res.*, 2003, **42**, 2427-2433.
- 49 S. Hao, H. Chang, Q. Xiao, Y. Zhong, W. Zhu, *J. Phys. Chem. C*, 2011, **115**, 12873-12882.
- 50 Z. Bacsik, R. Atluri, A.E. Garcia-Bennett, N. Hedin, *Langmuir*, 2010, **26**, 10013-10024.
- 51 N. Hiyoshi, K. Yogo, T. Yashima, *Chemistry Letters*, 2004, **33**, 510-511.
- 52 A. Danon, P.C. Stair, E. Weitz, *J. Phys. Chem. C*, 2011, **115**, 11540-11549.
- 53 O. Leal, C. Bolivar, C. Ovalles, J.J. Garcia, *Inorg. Chim. Acta*, 1995, **240**, 183-189.
- 54 M.L. Pinto, L. Mafra, J.M. Guil, J. Pires, J. Rocha, *Chemistry of Materials*, 2011, **23**, 1387-1395.
- 55 J.K. Moore, M. A. Sakwa-Novak, W. Chaikittisilp, A. K. Mehta, M. S. Conradi, C. W. Jones, S. E. Hayes, *Environ. Sci. Technol.* 2015, **49**, 13684-13691.
- 56 N. Hiyoshi, K. Yogo, T. Yashima, *Microp. Mesop. Mater.*, 2005, **84**, 357.

- 57 F. Zheng, D. Tran, B. Busche, G. Fryxell, R. Shane Addleman, T. Zemanian, C. Aardahl, *Ind. Eng. Chem. Res.*, 2005, **44**, 3099.
- 58 C. Knofel, J. Descarpentries, A. Banzaouia, V. Zelenak, S. Mornet, P.L. Llewellyn, V. Hornebecq, *Microporous and Mesoporous Materials*, 2007, **99**, 79-85.
- 59 C. Knofel, C. Martin, V. Hornebecq, P.L. Llewellyn, *J. Phys. Chem. C*, 2009, **113**, 21726-21734.
- 60 F. Brandani, D.M. Ruthven, C.G. Coe, *Industrial & Engineering Chemistry Research*, 2003, **42**, 1451 - 1461.